Chapter 14

Dynamic MRI of Small Electrical Activity

Allen W. Song, Trong-Kha Truong, Marty Woldorff

Abstract

Neuroscience methods entailing in vivo measurements of brain activity have greatly contributed to our understanding of brain function for the past decades, from the invasive early studies in animals using single-cell electrical recordings, to the noninvasive techniques in humans of scalp-recorded electroencephalography (EEG) and magnetoencephalography (MEG), positron emission tomography (PET), and, most recently, blood oxygenation level-dependent (BOLD) functional magnetic resonance imaging (fMRI). A central objective of these techniques is to measure neuronal activities with high spatial and temporal resolution. Each of these methods, however, has substantial limitations in this regard. Single-cell recording is invasive and only typically records cellular activity in a single location; EEG/MEG cannot generally provide accurate and unambiguous delineations of neuronal activation spatially; and the most sophisticated BOLD-based fMRI methods are still fundamentally limited by their dependence on the very slow hemodynamic responses upon which they are based. Even the latest neuroimaging methodology (e.g., multimodal EEG/fMRI) does not yet unambiguously provide accurate localization of neuronal activation spatially and temporally. There is hence a need to further develop noninvasive imaging methods that can directly image neuroelectric activity and thus truly achieve a high temporal resolution and spatial specificity in humans. Here, we discuss the theory, implementation, and potential utility of an MRI technique termed Lorentz effect imaging (LEI) that can detect spatially incoherent yet temporally synchronized, minute electrical activities in the neural amplitude range (microamperes) when they occur in a strong magnetic field. Moreover, we demonstrate with our preliminary results in phantoms and in vivo, the feasibility of imaging such activities with a temporal resolution on the order of milliseconds.

Key words: BOLD, fMRI, neuroimaging, noninvasive, Lorentz effect.

1. Introduction

Over the years, functional neuroimaging research has seen tremendous progress and greatly improved our understanding of brain function. The continuous pursuit to better measure neural activity has led to many exciting technical advances, including

Fahmeed Hyder (ed.), *Dynamic Brain Imaging: Multi-Modal Methods and In Vivo Applications, vol. 489*

DOI 10.1007/978-1-59745-543-5_14 Springerprotocols.com

single-cell electrical recordings, electroencephalogram (EEG), magnetoencephalogram (MEG), positron emission tomography (PET), and most recently, functional magnetic resonance imaging (fMRI). To date, however, these techniques are either invasive or limited in their ability to accurately localize neural activities in space or in time. Even when the latest multimodal neuroimaging methodology is used, there remain fundamental limitations that introduce sources of error and interpretative difficulties. For example, the simple combination of EEG (which has a high temporal resolution) and fMRI (which has a high spatial resolution) does not generally provide an unambiguous delineation of the spatiotemporal sequence of functional brain activity.

Among all the neuroimaging methods currently available, fMRI *(1–4)* has experienced a particularly explosive growth in recent years. The noninvasive nature of magnetic resonance imaging (MRI), along with its high apparent spatial resolution and moderate temporal resolution, rapidly engendered its emergence as one of the dominant techniques in functional brain research. Just about all of the fMRI contrast mechanisms developed thus far, however, have relied on indirect measures of neuronal activity. For example, the widely used blood oxygenation level dependent (BOLD) contrast relies on relative oxygenation changes, perfusion contrast relies on cerebral blood flow (CBF) changes, and cerebral blood volume (CBV) contrast relies on task-induced vessel expansion. Yet, none of the activities that these techniques measure are themselves thought to mediate information processing in the brain, but rather are hemodynamic ramifications of the neuronal activity itself. The hemodynamic modulations inevitably disperse the observed functional signal change both spatially and temporally, despite the high apparent spatiotemporal resolution of these techniques *(5, 6)*. Ideally, one would want to bypass these indirect markers and measure the activity of neurons directly. Motivated by the many advantages of MRI ideal for investigating brain function, researchers in the MR community have thus begun exploring and extending its use with the goal of being able to directly image transient neuronal activities.

Thus far, however, this type of direct MRI technique, albeit theoretically conceivable and probably the most intriguing, has still remained largely unattainable. The goal of noninvasive detection of neuroelectric activity with high spatiotemporal resolution has been extraordinarily challenging in the context of neuroimaging, as the electrical activity of neuronal tissue is extremely weak and the imaging voxels quite small. Indeed, even direct intracranial recordings of evoked local field potentials, which collectively acquire electrical signals from an area on the order of 1 cm^2, only measure potentials on the order of a few hundred microvolts and require hundreds of time-locked signal averages. Further, the electrical activities are also temporally transient and spatially

inhomogeneous, exacerbating the difficulties in direct imaging of neural activity using MRI. Nonetheless, theoretical models and initial experiments have been proposed and carried out, which have helped shed light on the tantalizing possibility of direct and noninvasive MRI of neurons in action.

An early MRI study in 1989 by Joy et al. *(7)* provided intriguing results. The authors used spin echo phase imaging to assess the magnetic field perturbations induced by externally injected electrical currents, both in phantoms and in vivo. Their results showed that electrical currents in biological systems on the order of milliamperes could be detected by acquiring phase maps during stimulation. Since neuronal action potentials are essentially electrical depolarizations, these results suggested that it may be possible to image neuronal activity directly using MRI. It first appeared that the limitation was simply the low signal-to-noise ratio (SNR), which could be improved by using time-locked averaging of multiple trials, as is used in techniques such as event-related potential (ERP/EEG) and event-related field (ERF/MEG) recordings and with event-related BOLD fMRI. However, many technical challenges arose in addition to the SNR limitations, including the spatially incoherent and temporally transient nature of the neuroelectric activity, and the multiple confounding synchronized signals reflecting BOLD, CBV, and CBF changes or physiological noise. These proved to be extremely difficult to address, and as a result there were virtually no breakthroughs in the decade following the initial demonstration.

Nevertheless, interest was renewed in the late 1990's after a decade of explosive fMRI research based on the hemodynamic (e.g., BOLD) contrasts. While researchers across various disciplines continue to be deeply attracted to such fMRI methods, neuroscientists and physicists have relatively quickly reached their intrinsic spatiotemporal limitations to truly interpret the neural activities. Several groups have thus recently assessed the feasibility of using MRI for direct imaging of neuronal activation, more specifically by attempting to detect the minute magnetic field changes induced either by electrical currents in phantoms *(8–10)* or by neuronal currents during evoked or spontaneous brain activity in cell cultures or human subjects *(11–22)*. Despite some encouraging results, many issues remain controversial. For example, several simulations *(10, 15)* and experimental *(14, 17)* studies have shown that phase images are more sensitive to magnetic field changes induced by neuronal currents than are magnitude images, yet others claim the opposite *(12, 20, 21)*. Furthermore, several attempts at reproducing the positive results obtained in earlier studies have been unsuccessful *(13, 22)*. Whether conclusive or not, all of these studies were intrinsically limited by the small magnitude of the magnetic field changes induced by neuronal activation. Moreover, and probably more importantly, they

did not take advantage of the strong main magnetic field and high-power gradient systems of modern MRI scanners.

To boost the signal detectability, we propose a new MRI technique termed Lorentz Effect Imaging (LEI) *(23, 24)*, which uses magnetic field gradients to significantly amplify and detect the Lorentz effect induced by spatially incoherent yet temporally synchronized neural-range electrical activity in a strong magnetic field. In the present work, we demonstrate its feasibility for imaging electrical currents on the order of microamperes with a temporal resolution on the order of milliseconds in gel phantoms and in vivo *(24, 25)*.

2. Theory

The LEI technique relies on the well known Lorentz effect, whereby a current-carrying conductor (or individual ions) exposed to a magnetic field experiences a Lorentz force equal to the cross product of the current vector (or electric charge) and the magnetic field. If the conductor (or individual ions) is surrounded by an elastic medium, this force induces a spatially incoherent displacement of the elastic medium in adjacent regions, resulting in a spatially incoherent displacement of the spins in these regions. In the presence of a magnetic field gradient, these spins experience a loss of phase coherence, which in turn results in a destructive signal summation within a voxel and, thus, a signal decay similar to that seen in the transverse relaxation effect. This contrast mechanism remains valid even for randomly oriented electrical current, or ionic flows, within a voxel, as the resultant spatially incoherent displacement of surrounding media (e.g. water molecules) still leads to a destructive signal summation, as shown in our recent manuscript *(26)*.

Since a magnetic field gradient also induces a loss of phase coherence of the static spins, resulting in an unwanted signal attenuation outside the regions of interest, balanced gradients (with positive and negative lobes of the same amplitude and duration) need to be applied, so that the phase shifts experienced by the static spins are rephased, as in diffusion-weighted imaging. These gradients must then be synchronized with the current such that it occurs only during either the positive or the negative lobe in order to preserve the phase shifts due to the Lorentz force-induced displacement. Furthermore, multiple cycles of such synchronized oscillating gradients can be used to greatly amplify the loss of phase coherence due to the Lorentz effect, and therefore increase the sensitivity of the technique. In this work, we use a gradient echo sequence with a series of oscillating gradients applied between excitation and data acquisition (**Fig. 14.1**).

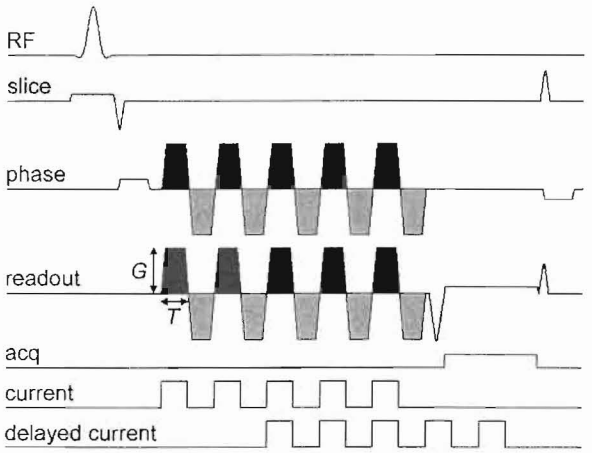

Fig. 14.1. Pulse sequence diagram for the phantom experiments. Gradient echo sequence with n (in this example, 5) cycles of oscillating magnetic field gradients (with positive and negative lobes of amplitude G and duration T, shown in *dark* and *light gray*) applied in the readout and phase encoding directions between excitation and data acquisition. The current is synchronized with the pulse sequence such that it is on only during the positive lobes of the oscillating gradients. In the third study (*bottom line*), the current is delayed with respect to the oscillating gradients (in this example, by two cycles).

Though LEI effect applies to ionic flows *(26)* and is not limited to a wire model, here we use the following simple model to help provide insight into the contrast mechanism of the LEI technique. Here, we consider a cylindrical current-carrying conductor oriented along the y axis, placed in a magnetic field oriented along the z axis, and surrounded by a homogeneous, isotropic, and linear elastic medium (**Fig. 14.2**). The resulting

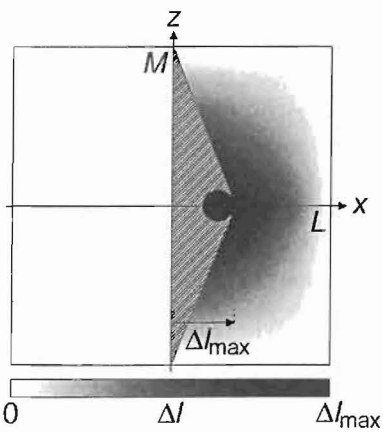

Fig. 14.2. A basic model of the signal loss. A current-carrying conductor (*black circle*) orthogonal to the plane of the figure, placed in a magnetic field oriented along the z axis, and surrounded by a linear elastic medium, experiences a Lorentz force resulting in a spatially incoherent displacement $\Delta l(x, z)$ of the elastic medium in the x direction ranging between 0 and Δl_{max}. It is assumed that there is no displacement in the $\{x < 0\}$ region and that there is an empty space in the hatched region (see text).

Lorentz force, oriented along the x axis and proportional to the current and the magnetic field, induces a displacement Δl_{max} of the conductor in the x direction, leading to a spatially incoherent displacement $\Delta\ l(x, z)$ of the surrounding elastic medium in the x direction. We assume that the deformation is elastic, i.e., the displacement is proportional to the applied force and inversely proportional to the Young's modulus of the elastic medium (Hooke's law). Furthermore, we assume that the conductor does not adhere to the elastic medium, so that it only induces a compression of the elastic medium on one side, but no dilation on the opposite side, thus leaving an empty space behind it. Because of the symmetry with respect to the z axis, we consider only the $\{z \geq 0\}$ region from now on. The maximum displacement experienced by the elastic medium is equal to the displacement of the conductor Δl_{max} and occurs at ($x = \Delta l_{max}$, $z = 0$). As a first order approximation, we assume that:

1. *(1)* There is no displacement in the $\{x \leq 0\}$, $\{x \geq L\}$, and $\{z \geq M\}$ regions (where L and M are defined in **Fig. 14.2**);
2. There is an empty space in the $\{0 < x < \Delta l_{max}(M-z)/M\}$ region (hatched in **Fig. 14.2**); (3) The displacement Δl at an arbitrary point (x, z) in the $\{\Delta l_{max}(M-z)/M \leq x \leq L\}$ region decreases linearly from Δl_{max} to zero as follows:

$$\Delta l(x, z) = \frac{L - x}{L - \Delta l_{\max}\frac{M-z}{M}} \frac{M - z}{M} \Delta l_{\max} \tag{14.1}$$

In this region, the spin density is therefore equal to

$$\rho'(z) = \rho \frac{L}{L - \Delta l_{\max}\frac{M-z}{M}}, \tag{14.2}$$

where ρ is the spin density in the absence of Lorentz force, and the phase shift obtained by applying n cycles of oscillating gradients (whose positive lobes are synchronized with the current) along the x axis is given by

$$\phi(x, z) = \gamma\, n \int_0^T G\, \Delta l(x, z)\, \mathrm{d}t \approx \gamma\, n\, G\, T\, \Delta l(x, z), \tag{14.3}$$

where G and T are the amplitude and duration of one gradient lobe respectively, and γ is the gyromagnetic ratio ($2\pi \times 42.57 \times 10^6$ rad/T for protons). This phase shift is thus directly proportional to the displacement. To derive the right-hand side of **Equation (14.3)**, the displacement was assumed to occur over a time much shorter than T. If this were not the case, the resulting phase shift would be smaller.

The ratio of the signal intensity with and without Lorentz effect in a voxel of dimensions $L \times M$ can be computed by integrating the phase shift over the $\{0 \leq x \leq L; 0 \leq z \leq M\}$ region:

$$R = \frac{\sqrt{\left[\int_0^M \int_{\Delta l_{\max}(M-z)/M}^{L} \rho'(z)\cos\phi(x,z)\,dx\,dz\right]^2 + \left[\int_0^M \int_{\Delta l_{\max}(M-z)/M}^{L} \rho'(z)\sin\phi(x,z)\,dx\,dz\right]^2}}{\int_0^M \int_0^L \rho\,dx\,dz}$$

$$= \frac{1}{|\phi_{\max}|}\sqrt{\left(\int_0^{\phi_{\max}} \frac{\sin\alpha}{\alpha}d\alpha\right)^2 + \left(\int_0^{\phi_{\max}} \frac{1-\cos\alpha}{\alpha}d\alpha\right)^2}, \quad (14.4)$$

where $\phi_{max} = \phi(\Delta l_{max})$. Because of the complex nature of the compression of the elastic medium, the derivation of an analytical solution for a more general case is more difficult. Nevertheless, the simplified model developed here does give an insight into the signal loss mechanism of the LEI technique, while also providing a preliminary theoretical foundation for the quantitative evaluation of small electrical activity-induced MR signal changes as a function of the spatially incoherent displacement.

3. Methods

Building upon this initial theoretical analysis, phantom and in vivo experiments were designed and carried out to examine the contrast mechanism of the LEI technique, demonstrate its high spatial and temporal resolution, and assess its sensitivity for potential applications in biological systems.

3.1. Phantom Experiments

Two spherical gel phantoms (diameter 10 cm, 2.2% gelatin) were constructed. Phantom A contained a straight bundle of carbon wires (overall diameter 500 μm), whereas phantom B contained ten wires (diameter 100 μm) connected in parallel and oriented in random directions in three dimensions. The wires were connected via shielded cables to a square-wave pulse generator triggered by the positive lobes of the oscillating gradients, with a large resistor ($> 1K\Omega$) connected in series to minimize any current induced by the switching gradients that could contribute to the Lorentz effect.

All experiments were performed on a 4 T whole-body MRI scanner (General Electric Medical Systems, Milwaukee, WI, USA) equipped with a high power gradient system (40 mT/m maximum amplitude, 150 T/m/s slew rate), using a shielded quadrature birdcage head coil. The acquisition parameters were optimized based on the following considerations. **Equation (14.3)** shows that large values for n, G, and T should be used to amplify the loss of phase coherence and thus the resulting signal decay due to the Lorentz force-induced displacement. However, the increased diffusion weighting, quantified by the following b-factor: $b = (2/3)\,n\gamma^2 G^2 T^3$ (for one gradient axis) *(27)*, would result in a global signal attenuation. Since the phase

shift is proportional to n, G, and T, whereas the b-factor is proportional to n, G^2, and T^3, it is preferable to use strong and short, rather than weak and long, gradient oscillations, as well as a large number of short gradient oscillations rather than fewer long ones. Consequently, we chose $G = 40$ mT/m and $T = 2$ ms. Furthermore, another trade-off for using a large number of gradient oscillations is the increased echo time (TE) needed to accommodate these gradients, resulting in a global signal attenuation due to T_2^* relaxation. We, therefore, experimentally determined that a value of $n = 15$, corresponding to a minimum TE of 71 ms, was optimal. With this choice of parameters, a maximum displacement Δl_{max} of 10 μm would result in a maximum phase shift $\phi_{max} \approx \pi$ and a signal loss $R \approx 20\%$, as estimated from Equations (14.3) and (14.4) respectively. The resulting b-factor is only 9 s/mm^2, thus causing a negligible signal attenuation due to diffusion weighting. Other imaging parameters were chosen as follows: Repetition time 1000 ms, flip angle 70°, field-of-view 12 cm, matrix size 256 × 128, and slice thickness 5 mm.

Three studies were carried out to assess the dependence of the LEI signal on the intensity of straight and randomly oriented electrical currents, as well as its dependence on the synchronization between the current and the oscillating gradients for a fixed current intensity.

The first study was conducted on phantom A to evaluate the sensitivity of the LEI technique using the simplest geometry. The phantom was positioned in the magnet with the wire orthogonal to the main magnetic field to maximize the Lorentz effect. Axial images were acquired with oscillating gradients applied in the direction orthogonal to both the wire and the main magnetic field, since the Lorentz force induced displacement occurs in that direction. Current pulses of 0, 5, 10, 20, 50, 100, 200, and 500 μA were applied in synchrony with the positive lobes of the oscillating gradients (in separate acquisitions), thus covering the range of values found in biological systems. Five averages were used for current intensities up to 20 μA to increase the SNR.

The second study was conducted on phantom B to demonstrate the feasibility of the LEI technique to detect currents flowing in multiple directions with a more complex geometry. All parameters were identical to those used in the first study, except that oscillating gradients were applied along both directions orthogonal to the main magnetic field. The LEI technique can detect displacements occurring in multiple directions whether oscillating gradients are applied along only one axis or both axes orthogonal to the main magnetic field. In either case, it is most sensitive to displacements occurring in the direction of the largest gradient. However, when oscillating gradients are applied along both axes rather than only one axis, this largest gradient is a factor $\sqrt{2}$ larger (assuming they have the same amplitude along both axes), and consequently the overall sensitivity is higher.

The third study was carried out for two purposes: First, to confirm that the observed signal loss is predominantly due to the intravoxel dephasing resulting from the spatially incoherent displacement of the gel rather than to the bulk displacement of the wire itself (as the wire does not generate any MR signal); and second, to demonstrate the high temporal resolution of the LEI technique. In this experiment, the current intensity was set at 500 μA and the current pulses were delayed with respect to the positive lobes of the oscillating gradients by 0–15 cycles, resulting in an overlap of 15–0 cycles between the two, respectively (**Fig. 14.1**, bottom line). As such, the Lorentz force induced displacement remained identical throughout the study, while the amount of loss of phase coherence and resulting signal decay due to the incoherent displacement was systematically varied. The study was conducted on phantom A with all other parameters identical to those used in the first study. The image acquired with no overlap between the current and the oscillating gradients (in which no signal change should occur) served as the reference, and, as such, was acquired using five averages to increase the SNR.

While the above experiments demonstrate LEI effect in a wire model, similar phenomenon is observed in ionic conductions in our recent work *(26)*, with LEI effect further amplified by the surrounding water molecules. This solution model of the LEI effect may be better suited to simulate the neural conductions in vivo.

4. In vivo *Experiments*

The concept of using synchronized oscillating gradients to increase the signal detectability from electrical currents was extended to in vivo experiments. To minimize potential confounds from hemodynamic modulations or physiological noise commonly seen in brain activation studies and ensure a precise timing control on the stimuli, these experiments were performed in the human median nerve by using electrical stimulation of the wrist to induce intrinsic sensory compound nerve action potentials.

Electrical stimulation of the median nerve was accomplished with a high-impedance electrical current stimulator (Grass S12; Grass-Telefactor, West Warwick, RI, USA) and two gold-plated disk electrodes secured on the ventral and dorsal sides of the right wrist directly over the median nerve (Note: Identical results were obtained when both electrodes were placed on the ventral side of the wrist directly over the median nerve). The current was delivered through the filtered penetration panel via shielded and twisted cables, with the shield grounded to the panel. All electrical switches were installed outside the magnet room, effectively isolating the electrical stimulation in the magnet room and thus

removing any electrical interference with the MRI signal. The stimuli consisted of a series of biphasic rectangular current pulses with a duration of 1 ms and an amplitude ranging from 1.8 to 2.7 mA, which was set prior to each session to be just below the motor threshold for finger movement in order to avoid motion artifacts (electromyography measurements were performed for confirmation). The stimulator was triggered by the MRI scanner to ensure an accurate synchronization between the electrical stimulation and the pulse sequence.

The studies were performed on the same 4 T whole-body MRI scanner as used for the phantom experiments. All images were acquired by using a surface coil designed in-house and a gradient echo single-shot spiral imaging sequence with the following parameters: Repetition time 2,000 ms, TE 35.5 ms, flip angle 80°, field-of-view 20 cm, matrix size 64 × 64, and three contiguous axial slices (sagittal with respect to the forearm), which were each 15 mm thick and centered on the median nerve to ensure that the section of the nerve between the wrist and the elbow would be fully contained within one slice. A series of oscillating gradients with an amplitude of 36 mT/m and a duration of 5 ms for each lobe was applied along both axes orthogonal to the main magnetic field. Because the conduction time of the sensory activation in the human median nerve between the wrist and the elbow is about 4 ms *(28)*, this duration of 5 ms was chosen to ensure that sensory nerve action potentials could propagate in that section of the nerve within one lobe. High-resolution T_1-weighted images were also acquired at the same location for anatomical reference.

Four experiments were performed to examine the signal changes during stimulation. To ensure sufficient loss of phase coherence while limiting the T_2^* decay, a maximum of three cycles of gradient oscillations and three synchronized electrical pulses was used for the first experiment (Exp. 1, **Fig. 14.3a**). To establish a graded effect, a second experiment was carried out with only two cycles of gradient oscillations and two synchronized electrical pulses (Exp. 2, **Fig. 14.3b**). In addition, two control experiments were performed that were identical to Exp. 1 but with the electrical pulses delayed by 50 ms with respect to the oscillating gradients (Exp. 3, **Fig. 14.3c**) or without oscillating gradients (Exp. 4, **Fig. 14.3d**).

The activation paradigm was a block design consisting of seven alternating rest and stimulation periods, each lasting 20 seconds, during which ten image volumes were acquired. During the stimulation periods, electrical pulses were triggered to excite the median nerve, whereas during the rest periods, no stimulation was applied. Four runs were acquired for each experiment and averaged to increase the SNR.

After each run, subject bulk motion was assessed by computing the displacement of the image center-of-mass over time slice-by-slice, and runs with an in-plane displacement exceeding

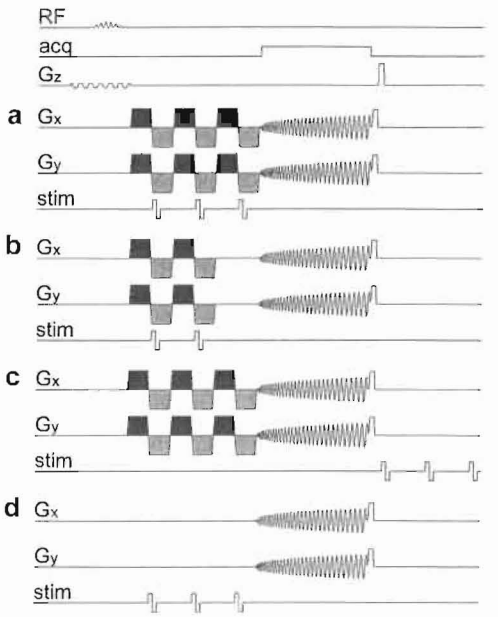

Fig. 14.3. Pulse sequence diagrams for the in vivo experiments. Timing of the radiofrequency excitation pulse (RF), the data acquisition window (acq), the magnetic field gradients on the slice selection (G_z), readout (G_x), and phase encoding (G_y) axes, and the current applied by the stimulator to the wrist (stim) for: (**a**) Three cycles of gradient oscillations (shown in *dark* and *light gray*) and three electrical pulses triggered at the onset of the negative gradient lobes (Exp. 1); (**b**) the same as (**a**) but with two cycles of gradient oscillations and two electrical pulses (Exp. 2); (**c**) the same as (**a**) but with the electrical pulses delayed by 50 ms (Exp. 3); (**d**) the same as (**a**) but without oscillating gradients (Exp. 4).

one pixel were discarded ($\sim 10\%$ of the runs). Voxel-by-voxel linear detrending was applied to remove any linear drift in the MRI signal. A group student's t-test (one-tailed) was then carried out to detect significant differences between the images acquired during the rest and stimulation periods. The t-score maps were converted to Z-score maps and thresholded using a Z-score of $Z > 5$ (corresponding to a significance level of $P < 2.5 \times 10^{-7}$ uncorrected for multiple comparisons) and a cluster size of five voxels. Finally, the resulting activation maps were overlaid on the coregistered high-resolution anatomical images.

5. Results

5.1. Phantom Experiments

5.1.1. Current Intensity Dependence for a Straight Current

The results of the first phantom study are shown in **Fig. 14.4**. As expected, the central signal dip observed on the image acquired without current (**Fig. 14.4a**), which is due to the presence of the wire, becomes progressively larger and wider with increasing current intensities, as can be seen more clearly on the difference images (**Fig. 14.4b**). This signal loss, caused by the intravoxel

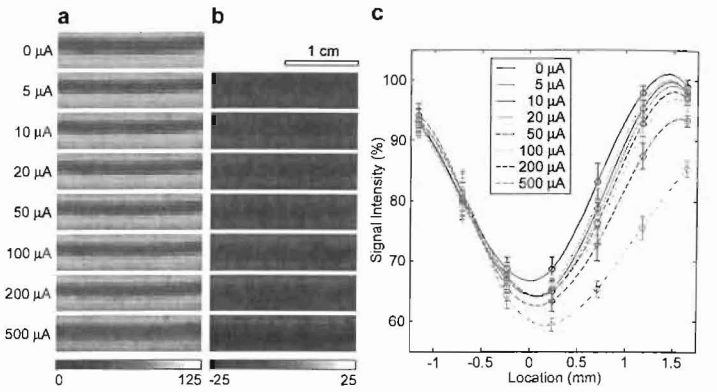

Fig. 14.4. Current intensity dependence for a straight current. (**a**) Images of a selected region of phantom A containing the wire acquired with different current intensities. (**b**) Corresponding difference images with the image acquired without current. (**c**) Signal intensity profiles across the wire averaged over the section shown in (**a**) and (**b**) for the different current intensities. The lines are computed using cubic spline interpolation. The signal intensity in (**a**), (**b**), and (**c**) is expressed in percentage of the maximum signal in the image acquired without current.

dephasing due to the Lorentz force induced incoherent displacement, occurs only on one side of the wire, as shown on the plot of the average signal intensity profiles across the wire (**Fig. 14.4c**). Similar results are obtained when the direction of the current is reversed, except that the signal loss occurs on the opposite side. The widening can reach up to 750 μm (full width at half maximum) for a current intensity of 500 μA, with a corresponding maximal signal loss of 25%. However, currents as low as 5 μA can still be detected.

Although the signal loss was only observed on one side of the wire, since the latter does not adhere to the gel, it is important to note that even if this were not the case (e.g., for a neuron surrounded by tissue), a dilation of the elastic medium on the opposite side would induce a spatially incoherent displacement as well, and thus, a loss of phase coherence similar to that induced by the compression of the elastic medium, resulting in a signal loss on both sides and making the technique more sensitive.

5.1.2. Current Intensity Dependence for Randomly Oriented Currents

The results of the second phantom study are shown in **Fig. 14.5** and demonstrate that the LEI technique does not require unidirectional currents. As for the straight wire in the first study, the signal losses correspond to the wire locations and become more pronounced with increasing current intensities, which can be clearly seen on both the original images (**Fig. 14.5a**) and the difference images (**Fig. 14.5b**). The overall signal loss dependence on the current intensity is highly comparable to that observed for the straight current. However, because of the directional dependence of the LEI signal, the segments of wire that were

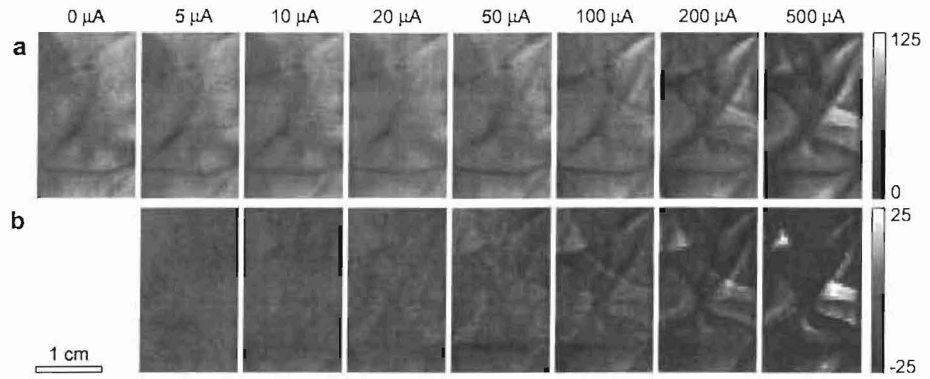

Fig. 14.5. Current intensity dependence for randomly oriented currents. (**a**) Images of a selected region of phantom B acquired with different current intensities. (b) Corresponding difference images with the image acquired without current. The signal intensity is expressed in percentage of the maximum signal in the image acquired without current.

not orthogonal to the main magnetic field experienced a smaller Lorentz force and therefore a smaller signal loss.

5.1.3. Dependence on the Synchronization between the Current and the Oscillating Gradients

The results of the third phantom study are shown in **Fig. 14.6** As expected, the signal loss progressively increases with the amount of overlap between the current pulses and the positive lobes of the oscillating gradients, which can be clearly seen on both the difference images (**Fig. 14.6b**) and the plot of the average signal loss within the entire region (**Fig. 14.6c**).

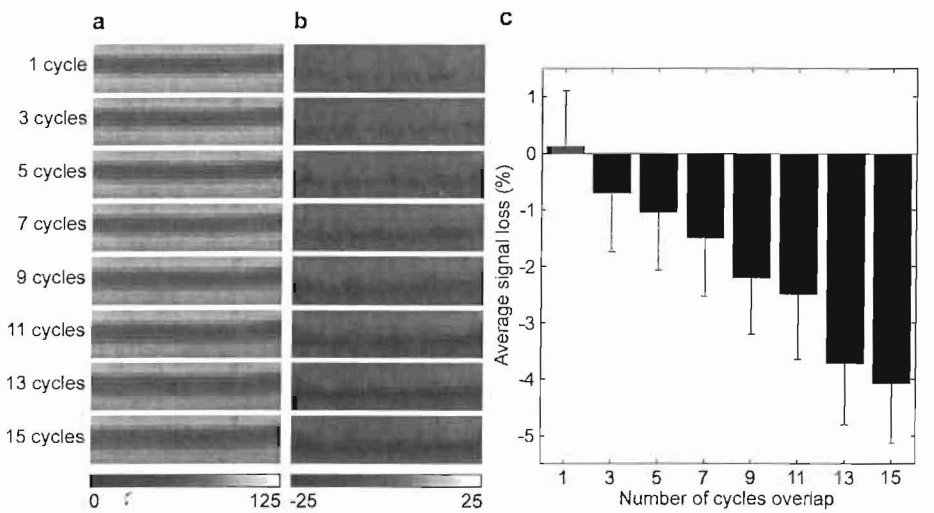

Fig. 14.6. Dependence on the synchronization between the current and the oscillating gradients. (**a**) Images of a selected region of phantom A containing the wire acquired with a 500 μA current intensity and different amounts of overlap between the current pulses and the positive lobes of the oscillating gradients. (**b**) Corresponding difference images with the image acquired without overlap, illustrating the signal loss as a function of the intravoxel dephasing, but not of the displacement itself. (**c**) Signal loss averaged over the region shown in (**a**) and (**b**) for the different amounts of overlap. The signal intensity in (**a**), (**b**), and (**c**) is expressed in percentage of the maximum signal in the image acquired without overlap.

In this study, the current intensity was fixed, so that the Lorentz force induced displacement remained identical for all conditions. On the other hand, the overlap between the current and the oscillating gradients was systematically varied, resulting in different amounts of loss of phase coherence. As such, these results demonstrate that the observed signal loss is predominantly due to the intravoxel dephasing resulting from the spatially incoherent displacement of the gel rather than the bulk displacement of the wire itself. Indeed, the signal loss from the bulk displacement itself is virtually undetectable as shown in the first image in **Fig. 14.6**, where only one cycle of overlap was used.

Furthermore, since the duration of one cycle of oscillating gradients is only 4 ms, these results also demonstrate that a temporal resolution on the order of milliseconds can be achieved with the LEI technique, which represents a dramatic improvement – at least two orders of magnitude – as compared to conventional BOLD fMRI.

5.2. *In vivo Experiments*

Figure 14.7 shows a representative functional activation map for Experiment 1, in which three cycles of gradient oscillations and three synchronized electrical pulses were used, overlaid on high-resolution T_1-weighted images of the forearm. Highly significant activation was found along the median nerve across subjects. The time course averaged over the activated region shows a systematic signal decrease of $(4.4 \pm 0.7)\%$ during the stimulation periods (**Fig. 14.8a**). The transitions between rest and stimulation periods exhibit no delay, in contrast to what is typically observed in conventional BOLD fMRI studies, which are limited by a hemodynamic delay of 3–6 seconds.

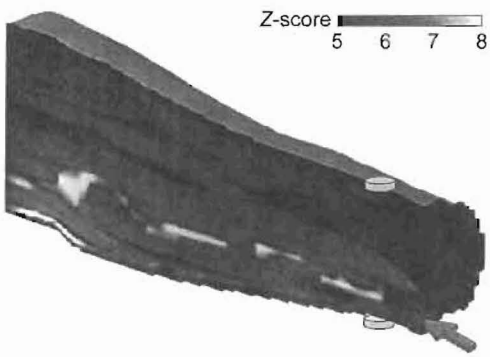

Fig. 14.7. Activation map showing the effect of neuroelectric activity in vivo in the human median nerve. The activation was obtained using three cycles of gradient oscillations and three electrical pulses synchronized with the negative gradient lobes (Exp. 1), and is overlaid on a stack of coregistered anatomical images. The discs represent the electrodes placed on the dorsal (*top*) and ventral (*bottom*) sides of the wrist. The arrow points to the median nerve.

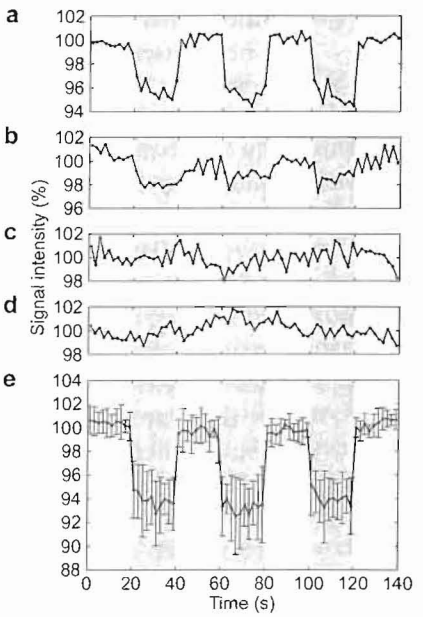

Fig. 14.8. Time courses during alternating periods of rest and electrical stimulation. These results were obtained using: (**a**) Three cycles of gradient oscillations and three electrical pulses synchronized with the negative gradient lobes (Exp. 1); (**b**) the same as (**a**) but with two cycles of gradient oscillations and two electrical pulses (Exp. 2); (**c**) the same as (**a**) but with the electrical pulses delayed by 50 ms (Exp. 3); (**d**) the same as (**a**) but without oscillating gradients (Exp. 4); (**e**) the same as (**a**) but averaged over seven different experimental sessions. The time courses in (**a–d**) were averaged over the activated region obtained in Experiment 1; the time course in (**e**) was averaged over the activated regions of all seven sessions. The error bars represent the standard deviation over the seven sessions. Each time course is normalized to the mean signal intensity during rest. The rest and stimulation periods are shown in white and gray, respectively.

Less significant activation was detected in Experiment 2, in which only two cycles of gradient oscillations and two synchronized electrical pulses were used. The time course averaged over the same activated region as in Experiment 1 shows a signal decrease of only $(1.5 \pm 0.6)\%$ during the stimulation periods (**Fig. 14.8b**). This finding illustrates that the sensitivity of our technique can be significantly decreased when there is insufficient loss of phase coherence, which is consistent with its contrast mechanism.

As expected, no activation was detected in either control experiment, in which the electrical pulses were delayed with respect to the oscillating gradients (Exp. 3) or in which no oscillating gradients were used (Exp. 4). The time courses averaged over the same activated region as in Experiment 1 show no systematic signal changes during the stimulation periods (**Figs. 14.8c and d**). These results further validate the contrast mechanism of our technique by demonstrating that the observed activation is indeed due to the loss of phase coherence generated

by the oscillating gradients rather than the bulk displacement of the nerve itself, since this displacement is present in both control experiments, but is not synchronized with oscillating gradients. It should thus be emphasized that the magnitude of the displacement does not by itself determine the sensitivity of the technique, since, for a given displacement, the loss of phase coherence can be independently amplified by using more, stronger, and/or longer oscillating gradients, given sufficient SNR. Furthermore, the fact that the loss of phase coherence can be amplified by the oscillating gradients demonstrates that it is indeed caused by the spatially incoherent displacement rather than the magnetic field induced by the current. Finally, Experiments 3 and 4 also show that there are no artifacts due to eddy currents induced in the stimulation circuit by the oscillating gradients or electrical interference from the stimulation pulses, respectively, since no activation was detected when oscillating gradients or electrical pulses were applied alone.

It can therefore be derived that Experiment 2 is equivalent to Experiment 1 but with a one-cycle (i.e., 10 ms) temporal offset between the electrical stimulation and the oscillating gradients, since only electrical pulses that are synchronized with oscillating gradients contribute to the observed activation. As such, the significant difference between the results of Experiments 1 and 2 shows that our technique is sensitive to timing differences of the stimulation paradigm on the order of milliseconds, thus demonstrating its high temporal resolution.

Finally, to evaluate the test-retest reliability of our technique for directly imaging neuroelectric activity in vivo in a healthy median nerve, Experiment 1 was carried out in seven separate sessions on the same subject under identical experimental conditions to remove the dependence on subject and experimental variability. Highly significant activation was consistently detected along the median nerve in each session. The time course in the activated regions averaged over the seven sessions (**Fig. 14.8e**) highly resembles that obtained in a single session (**Fig. 14.8a**) and shows a systematic signal decrease of $(6.3 \pm 2.2)\%$ during the stimulation periods, confirming the consistency and robustness of our technique.

6. Discussion and Conclusions

The results presented here demonstrate the capability of the LEI technique for imaging spatially incoherent yet temporally synchronized electrical currents on the order of microamperes with a temporal resolution on the order of milliseconds. Accordingly, they provide a theoretical and experimental foundation

for its potential application in imaging neural activities in the human brain.

Our studies have shown that the sensitivity of the LEI technique can be substantially improved by applying successive cycles of oscillating gradients and using optimized parameters. Moreover, this sensitivity can be further increased by using a higher field strength (since not only the SNR but also the magnitude of the Lorentz effect increases with field strength) and/or stronger oscillating gradients, as such advances in hardware become increasingly more available on modern MRI scanners. This is a clear advantage relative to methods that rely on the intrinsic magnetic field changes induced by the current, which are independent of the main magnetic field strength.

As shown here in the human median nerve, the LEI technique can potentially be applied to white matter tracts in the central nervous system to study the functional connectivity between various brain areas and to assess white matter integrity in diseases such as multiple sclerosis. Further, since our technique does not require the electrical current to be unidirectional, it can potentially be extended to image focal dendritic neuroelectric activity in gray matter, which, if successful, could have a tremendous impact on our ability to noninvasively study neuronal information processing in the brain. However, unlike for applications in the peripheral nervous system, the temporal delays between the stimuli and the neural activation in various cortical areas are often not known, making it difficult to synchronize the pulse sequence with the neuroelectric activity. Nevertheless, scalp ERP recordings could be used to help determine the proper delays, which could then be incorporated into the pulse sequence to allow time-locked detection of neural activation.

Despite the promising results presented here, direct noninvasive neuroimaging in the human brain using the LEI technique remains experimentally challenging. First, synchronized confounding factors, such as functional signals reflecting BOLD, CBV, and CBF changes, as well as physiological noise, can dominate the detected signal. Therefore, a careful design of the experimental paradigm is required to separate these slow effects from the rapid effects due to neuroelectric activity. In addition, as mentioned above, the criticality of the close timing synchrony between the neuroelectric activity and the oscillating gradients will require considerable further development for this technique to work successfully in gray matter. Moreover, even if all the timing information is known (e.g., using ERP or other neuroelectrical data), the need for extremely accurate synchronization between the stimulation and image acquisition will be highly demanding on present hardware capabilities. Nevertheless, such efforts to overcome these challenges and implement our technique

for direct imaging of brain neuroelectric activity in vivo are currently underway.

With these challenges addressed, the potential of using LEI to directly and noninvasively image neural activations in real time can be realized to achieve both a high temporal resolution and spatial specificity as compared to conventional BOLD fMRI, and to help determine hierarchical organizations within activated neural networks. It is anticipated that, if even moderately successful, this technique could have a significant impact on neuroscience research.

Acknowledgments

This work was, in part, supported by the NIH (NS 50329, NS 41328) and NSF (BES 602529).

References

1. K.K. Kwong, J.W. Belliveau, D.A. Chesler, I.E. Goldberg, R.M. Weisskoff, B.P. Poncelet, D.N. Kennedy, B.E. Hoppel, M.S. Cohen, R. Turner, H.-M. Cheng, T.J. Brady, B.R. Rosen, Dynamic magnetic resonance imaging of human brain activity during primary sensory stimulation, Proc. Natl. Acad. Sci. USA 89 (1992) 5675–5679.
2. P.A. Bandettini, E.C. Wong, R.S. Hinks, R.S. Tikofski, J.S. Hyde, Time course EPI of human brain function during task activation, Magn. Reson. Med. 25 (1992) 390–397.
3. S. Ogawa, D.W. Tank, R. Menon, J.M. Ellermann, S.G. Kim, H. Merkle, K. Ugurbil, Intrinsic signal changes accompanying sensory stimulation: functional brain mapping with magnetic resonance imaging, Proc. Natl. Acad. Sci. USA 89 (1992) 5951–5955.
4. S. Ogawa, R.S. Menon, D.W. Tank, D.G. Kim, H. Merkle, J.M. Ellermann, K. Ugurbil, Functional brain mapping by blood oxygenation level-dependent contrast magnetic resonance imaging. A comparison of signal characteristics with a biophysical model, Biophys. J. 64 (1993) 803–812.
5. S.G. Kim, W. Richter, K. Ugurbil, Limitations of temporal resolution in functional MRI, Magn. Reson. Med. 37 (1997) 631–636.
6. R.L. Buckner, Event-related fMRI and the hemodynamic response, Hum. Brain Mapp. 6 (1998) 373–377.
7. M. Joy, G. Scott, M. Henkelman, In vivo detection of applied electric currents by magnetic resonance imaging, Magn. Reson. Imaging 7 (1989) 89–94.
8. J. Bodurka, A. Jesmanowicz, J.S. Hyde, H. Xu, L. Estkowski, S.J. Li, Current-induced magnetic resonance phase imaging, J. Magn. Reson. 137 (1999) 265–271.
9. J. Bodurka, P.A. Bandettini, Toward direct mapping of neuronal activity: MRI detection of ultraweak, transient magnetic field changes, Magn. Reson. Med. 47 (2002) 1052–1058.
10. D. Konn, P. Gowland, R. Bowtell, MRI detection of weak magnetic fields due to an extended current dipole in a conducting sphere: A model for direct detection of neuronal currents in the brain, Magn. Reson. Med. 50 (2003) 40–49.
11. H. Kamei, K. Iramina, K. Yoshikawa, S. Ueno, Neuronal current distribution imaging using magnetic resonance, IEEE Trans. Magn. 35 (1999) 4109–4111.
12. J. Xiong, P.T. Fox, J.H. Gao, Directly mapping magnetic field effects of neuronal activity by magnetic resonance imaging, Hum. Brain Mapp. 20 (2003) 41–49.
13. R. Chu, J.A. de Zwart, P. van Gelderen, M. Fukunaga, P. Kellman, T. Holroyd, J.H. Duyn, Hunting for neuronal currents: Absence of rapid MRI signal changes during visual-evoked response, Neuroimage 23 (2004) 1059–1067.
14. M. Bianciardi, F. Di Russo, T. Aprile, B. Maraviglia, G.E. Hagberg, Combination of BOLD-fMRI and VEP recordings for spin-echo MRI detection of primary magnetic effects caused by neuronal currents, Magn. Reson. Imaging 22 (2004) 1429–1440.

15. D. Konn, S. Leach, P. Gowland, R. Bowtell, Initial attempts at directly detecting alpha wave activity in the brain using MRI, Magn. Reson. Imaging 22 (2004) 1413–1427.
16. P.A. Bandettini, N. Petridou, J. Bodurka, Direct detection of neuronal activity with MRI: Fantasy, possibility, or reality?, Appl. Magn. Reson. 29 (2005) 65–88.
17. N. Petridou, D. Pleaz, A.C. Silva, M. Lowe, J. Bodurka, P.A. Bandettini, Direct magnetic resonance detection of neuronal electrical activity, Proc. Natl. Acad. Sci. USA 103 (2006) 16015–16020.
18. L.S. Chow, G.G. Cook, E. Whitby, M.N.J. Paley, Investigating direct detection of axon firing in the adult human optic nerve using MRI, Neuroimage 30 (2006) 835–846.
19. G.E. Hagberg, M. Bianciardi, B. Maraviglia, Challenges for detection of neuronal currents by MRI, Magn. Reson. Imaging 24 (2006) 483–493.
20. Y. Xue, J.-H. Gao, J. Xiong, Direct MRI detection of neuronal magnetic fields in the brain: Theoretical modeling, Neuroimage 31 (2006) 550–559.
21. L.S. Chow, G.G. Cook, E. Whitby, M.N.J. Paley, Investigation of MR signal modulation due to magnetic fields from neuronal currents in the adult human optic nerve and visual cortex, Magn. Reson. Imaging 24 (2006) 681–691.
22. L.M. Parkes, F.P. de Lange, P. Fries, I. Toni, D.G. Norris, Inability to directly detect magnetic field changes associated with neuronal activity, Magn. Reson. Med. 57 (2007) 411–416.
23. A.W. Song, A.M. Takahashi, Lorentz effect imaging, Magn. Reson. Imaging 19 (2001) 763–767.
24. T.-K. Truong, J.L. Wilbur, A.W. Song, Synchronized detection of minute electrical currents with MRI using Lorentz effect imaging, J. Magn. Reson. 179 (2006) 85–91.
25. T.-K. Truong, A.W. Song, Finding neuroelectric activity under magnetic-field oscillations (NAMO) with magnetic resonance imaging in vivo, Proc. Natl. Acad. Sci. USA 103 (2006) 12598–12601.
26. T.-K. Truong, A. Avram, A. W. Song, Lorentz effect imaging of ionic currents in solutions, J. Magn. Reson. 59 (2008) 221–227.
27. E.O. Stejskal, J.E. Tanner, Spin diffusion measurements: Spin echoes in the presence of a time-dependent field gradient, J. Chem. Phys. 42 (1965) 288–292.
28. J. Kimura, Electrodiagnosis in disease of nerve and muscle: Principles and practice, Oxford University Press, Oxford (2001).